Mathematical Biosciences and Engineering

MBE, 22(4): 962–987.
DOI: 10.3934/mbe.2025035
Received: 21 January 2025
Revised: 28 February 2025
Accepted: 04 March 2025
Published: 14 March 2025

https://www.aimspress.com/journal/MBE

Research article

Exploring brain dysfunction in IBD: A study of EEG-fMRI source imaging based on empirical mode diagram decomposition

Yujie Kang[1], Wenjie Li[1], Jidong Lv[1], Ling Zou[1,2,*], Haifeng Shi[3,*] and Wenjia Liu[3,*]

[1] School of Microelectronics and Control Engineering, Changzhou University, Changzhou 213164, China
[2] School of Medical and Health Engineering, Changzhou University, Changzhou 213164, China
[3] The Third Affiliated Hospital of Nanjing Medical University, Department of Radiology, Changzhou 213003, China

* **Correspondence:** Email: zouling@cczu.edu.cn, doctorstone771@163.com, 13813016290@126.com.

Abstract: Patients with inflammatory bowel disease (IBD) often suffer from mood disorders and cognitive decline, which has prompted research into abnormalities in emotional brain regions and their functional analysis. However, most IBD studies only focus on single-modality neuroimaging technologies. Due to a limited spatiotemporal resolution, it is unfeasible to fully explore deep brain source activities and accurately evaluate the brain functional connectivity. Therefore, we propose an electroencephalography (EEG)-functional magnetic resonance imaging (fMRI)source imaging method based on an empirical mode diagram decomposition (EMDD) and performed a synchronous EEG-fMRI source imaging analysis on 21 IBD patients and 11 healthy subjects. The high-frequency spatial components of the fMRI were extracted through EMDD as prior constraints and compared with the EEG source imaging based on the entire fMRI spatial prior. Then, the cortical source time series were reconstructed according to the Desikan-Killiany atlas for an effective connectivity analysis. The results showed that the EEG-fMRI source imaging based on EMDD had a better performance, with the average log model evidence increased by 29.60% and the average explained variance increased by 19.12%. There were significant differences in the activation intensity of a series of abnormal brain regions between IBD patients and healthy controls, some of which were newly discovered: the uncus, claustrum, lentiform nucleus, and lingual gyrus. Moreover, the findings from the effective connectivity analysis of cortical source signals revealed that IBD patients had information flow loss in the frontal lobes, central areas, left parietal lobe, and right temporal lobe, and the information flow intensity of the right lingual gyrus was enhanced.

Keywords: EEG source imaging; inflammatory bowel disease; EEG-fMRI fusion; empirical mode diagram decomposition; effective connectivity analysis

1. Introduction

Inflammatory bowel disease (IBD), including Crohn's disease (CD) and ulcerative colitis (UC), is a type of chronic intestinal inflammatory disease with relapses and remissions [1]. In addition to gastrointestinal symptoms, IBD is also associated with emotional and cognitive aspects. Emotional disorders and cognitive dysfunction may worsen the condition of IBD patients, and inflammation also affects the patient's emotional state and cognitive function [2]. It is not surprising that brain structures and functions closely related to emotions have become a major research focus due to their widespread impact on psychological, emotional, and physiological health.

Non-invasive brain imaging technologies play a crucial role in cognitive science research and clinical medical diagnosis. Functional magnetic resonance imaging (fMRI) is a non-invasive neuroimaging method that detects neural activity and functional changes in the brain using blood oxygen level dependent (BOLD) signals, thus offering high spatial resolution. Electroencephalography (EEG) is a non-invasive technique with high temporal resolution, which records the brain's electrical activity through scalp electrodes. At present, neuroimaging research on IBD mainly focuses on MRI research. Thomann et al. [3] employed multimodal data fusion techniques using structural magnetic resonance imaging (sMRI) and resting-state functional MRI (rs-fMRI) to investigate brain structure and function alterations in IBD. Their study found that IBD patients had structural changes in the frontal and temporal regions of the brain, and functional changes in the superior frontal gyrus, medial frontal gyrus, rectus gyrus, and subcingulate gyrus. Thapaliya et al. [4] studied the changes in the resting-state functional connectivity in active CD patients. They found that active CD patients had an increased connectivity in the frontoparietal and visual networks compared with healthy controls, alongside a decreased activity in the salience, default mode, and cerebellar networks. These changes may represent the neural correlates of chronic inflammation, abdominal pain, and severity.

However, EEG studies in IBD are relatively rare. Kelleci et al. [5] studied the prevalence of epileptic seizures and EEG abnormalities in CD patients and found that only one person in the CD patient group had the history of epilepsy and that the CD group had a significantly higher rate of EEG abnormalities, with the most common abnormality being intermittent slow waves at the θ rhythm. Kibleur et al. [6] first reported the central effects of vagus nerve stimulation (VNS) in CD patients. The study results showed that acute VNS could cause an increase in the spectral power of the δ and θ bands on the frontal, temporal, and occipital lobe electrodes; 12 months after chronic VNS, a decrease in α band power occurred. Apart from activating efferent vagal fibers, which regulat3e the autonomic nervous system, the study highlighted the regulatory effect of chronic VNS on anxiety and depression symptoms associated with CD through afferent vagal fibers.

The fusion of EEG and fMRI can provide a new method with high spatiotemporal resolution to study the brain structure and function [7]. The penetration depth of the EEG source localization is generally and comprehensively evaluated through multiple dimensions such as source localization accuracy, spatial resolution, and the comparison of inversion problem solving models. The effect of the penetration depth is usually reflected in the source localization accuracy and the ability to recognize signals from deep brain regions [8]. Reference [9] used a spontaneous power analysis of EEG-fMRI

to reveal differences in neural activity in the α and β bands between Sickle Cell Disease patients and healthy controls, thus indicating that EEG-fMRI source imaging has high spatial resolution and penetration depth and can detect changes in activity in deep brain regions. Some existing EEG source localization methods, such as weighted minimum norm estimation (wMNE) [10] and low-resolution brain electromagnetic tomography (LORETA) [11], have their own shortcomings. For example, compared with wMNE, LORETA localized the activity source of deep brain regions more smoothly and better, though it had a lower spatial resolution, which was not conducive to the brain source estimation [12]. In addition, some studies conducted a fMRI-constrained EEG source localization analysis, which limits the search space of the evoked potential neural source estimation to the cortical area identified by fMRI. Jiang et al. [13] proposed an EEG-fMRI source imaging method based on sparse optimization Bayes to study the brain activity in emotional decision-making problems. The source localization results obtained by this method were more concentrated and accurate. Sadjadi et al. [14] studied the localization of epileptic lesions through an EEG-fMRI source localization method based on the general linear model (GLM), thus providing a feasible solution for the preoperative evaluation of epilepsy patients. However, few studies have performed EEG-fMRI source imaging analyses of the brain structure and function of patients with IBD.

Most current studies on brain function and structure in IBD only used a single-modality approach. The abnormal brain regions and brain function analyses obtained in these studies were local and not comprehensive. The research results of single-modality fMRI are almost all about changes in the structure of superficial brain areas in IBD patients, such as changes in the gray matter volume in the frontal and temporal lobes, as well as changes in the functional connectivity between some brain areas. There is no comprehensive discovery of abnormal brain areas, including deep brain areas. The activity sources in deep brain regions are so difficult to detect that it is impossible to evaluate their impact on the brain function. EEG-fMRI source imaging studies can more comprehensively explore the abnormal brain regions in IBD patients and provide a basis for subsequent studies on functional changes in their abnormal brain regions. Although EEG offers a high temporal accuracy to reveal the dynamics of neural activities and potentially unearth brain sources, it suffers from poor spatial resolution and the problem of volume conduction, which may make the estimation of brain sources unreliable. To solve the problem of locating deep brain sources caused by the volume conduction effect, Moradi et al. [15] used the Fast and Adaptive Tridimensional Empirical Mode Decomposition (FATEMD) method to decompose the fMRI data and extract the high spatial frequency components as prior information for EEG source localization. The results showed that the localization accuracy of this source localization method was better than that of the EEG source localization using the entire fMRI activation map as a priori, and deep brain sources could be more accurately located. FATEMD is a three-dimensional extension of the Fast and Adaptive Bidimensional Empirical Mode Decomposition (FABEMD) [16]. It can decompose the volume into a set of three-dimensional intrinsic mode functions (TIMFs), the first TIMF being high frequency and the last one being low frequency. This method has opened up new paths for the three-dimensional extension of many applications.

On the other hand, fMRI has been extensively used to localize the active brain regions involved in emotional processing, though it is incapable of recovering accurate time courses of cortical activity and the accuracy of fMRI-based connectivity is questionable [17]. Recent research [18] has shown that correlation-based functional connectivity cannot depict the flow of influence between the brain regions, and the lack of influence direction poses difficulties in guiding model adjustments and in explaining the underlying functional mechanisms of brain work.

In light of these challenges, we propose a new EEG-fMRI source imaging method using the complementary information of EEG and fMRI signals in terms of the spatiotemporal resolution, namely a spatiotemporal constrained EEG-fMRI source imaging based on empirical mode diagram decomposition (EMDD). EMDD is a four-dimensional extension of FATEMD. It adds a time variable to the original decomposition of the three-dimensional volume, that is, it optimizes the number of iterations under specific time sequence conditions and can be used to decompose the fMRI data collected under multiple time sequences as a whole. Then, the decomposed fMRI high spatial frequency components are used to identify local high-intensity activations that are most likely to be captured by EEG, thereby reducing the impact of volume conduction effects and accurately finding the location of abnormal brain sources in IBD patients. In addition, we reconstruct the cortical source time series from the source space for an effective connectivity analysis. By studying the directional connectivity within the brain network of IBD patients, we aim to provide a theoretical basis to explore new indicators for clinical diagnoses and treatments.

2. Materials and methods

This study proposes a new EEG-fMRI source imaging method, namely a spatiotemporal constrained EEG-fMRI source imaging method based on EMDD. In a parametric Bayesian framework, this method can extract the fMRI high-frequency component Spatial Intrinsic Mode Functions (SIMF) through EMDD. Then, it performs an independent component analysis (ICA) on SIMF to obtain the resting-state network, constructs prior constraints, provides an accurate source reconstruction of the cortical activity, and performs an effective connectivity analysis on the reconstructed cortical activity time series.

The overall analysis scheme is summarized as follows (see Figure 1): (a) preprocess the 64-channel EEG data and extract the data in the "TREV" marked time period; (b) construct a three-layer real head model based on the subject's structural MRI data to calculate the guidance field matrix; (c) use the empirical mode graph decomposition algorithm to extract the high-frequency spatial component $SIMF_1$ in the fMRI data; (d) perform an ICA on $SIMF_1$ to identify and extract the resting state functional network in $SIMF_1$, including the default mode network, language network, and salience network, and construct a spatial prior; (e) use parametric empirical Bayesian inverse modeling to perform brain source imaging combined with time and space specific priors; and (f) perform an effective connectivity analysis on the reconstructed time series in the cortical source space to generate a brain network with causal relationships.

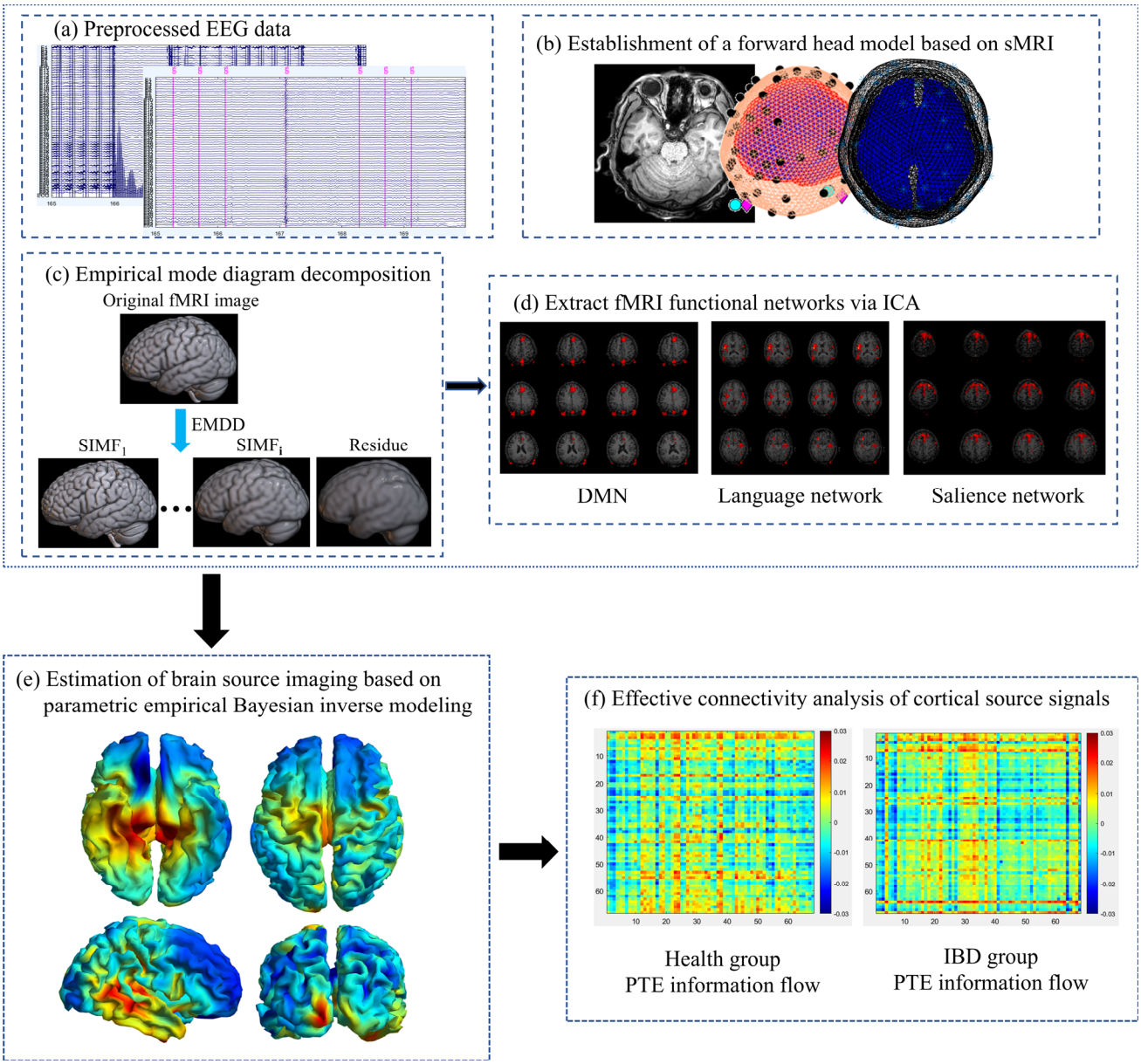

Figure 1. Scheme of overall data analysis process employed in this study. The 64-channel EEG data were preprocessed, and a three-layer realistic head model was constructed using the subject's structural MRI (sMRI) data. The EMDD algorithm was applied to the fMRI data to extract the high-frequency spatial component SIMF1, followed by an ICA to identify the resting-state functional networks, which were used to construct the spatial priors. Then, parametric empirical Bayesian inverse modeling was used for brain source imaging by integrating time- and space-specific priors. Finally, an effective connectivity analysis of the reconstructed cortical time series generated a causally connected brain network.

2.1. Participants

This study recruited 32 participants, including 21 IBD patients and 11 healthy controls, with an average age of (37.7 ± 15.4) years. All the participants were right-handed and received education.

The following exclusion criteria were applied: 1) use of corticosteroids and psychotropic medications within 30 days; 2) current or previous history of neurological, medical, or psychiatric disorders; 3) current or previous history of neurosurgery, head injury, cerebral vascular injury, or traumatic brain injury that involved a loss of consciousness; 4) presence of a learning disability; 5) presence of claustrophobia; 6) refusal to give informed consent; and 7) the presence of magnetic implants in the body.

All experimental procedures in this study were in accordance with the Declaration of Helsinki and approved by the ethics committee. All the participants signed informed consent before the experiment, and all methods were performed in accordance with the approved guidelines.

2.2. EEG-fMRI synchronous acquisition

The synchronous EEG-fMRI experiment was completed in the imaging department of a local hospital. The experiment was a resting-state experiment without eyes-opening or eyes-closing tasks, and the fMRI scanned 240 time points. The EEG acquisition equipment was a 64-lead magnetic resonance EEG signal acquisition system from the EGI Corporation in the United States. The electrode position followed the spatial distribution of the international 10-10 electrode system, and the central electrode was used as the reference. The sampling frequency was set to 250 Hz. The EEG acquisition software provided by EGI was used, which can display the collected EEG signals in real time, so as to observe the quality of the collected EEG signals in real time.

The magnetic resonance equipment was a 3.0 T superconducting functional magnetic resonance imaging system from Philips. The fMRI scanning parameters were as follows: repetition time (TR) of 2000 ms, echo time (TE) of 35 ms, field of view (FOV) of 230 mm × 180 mm, flip angle (FA) of 90°, layer thickness of 4 mm, and 24 layers were scanned continuously. The experiment adopted a scanning method of non-interval sequential scanning, and the "TREV" was marked in a 2 s time window in the fMRI scan. In the fusion experiment, a clock synchronization box was used to synchronize the time of the EEG and fMRI data acquisition.

2.3. Data preprocessing

The collected EEG data in the resting state were preprocessed on the EEGLAB [19] software. When the EEG and fMRI data are synchronously collected, there are roughly three sources of interference in the nuclear magnetic resonance environment. The first is the high-frequency interference introduced by the radio frequency transmitting coil, the second is the electrocardiogram artifact caused by the subject's heartbeat, and the third is the gradient artifact caused by the alternating gradient magnetic field. The strong magnetic field gradient switching in the scanner will bring strong gradient field artifacts to the EEG signal and the amplitude of the gradient field artifacts is much larger than the real scalp EEG signal, so it will cover the original EEG signal. The high-frequency interference introduced by the radio frequency transmission coil is much higher than the EEG signal frequency and is filtered out using a low-pass filter. ECG artifacts are collected through an additional ECG channel because of their fixed waveform, which can detect QRS complexes, and finally removed by FMRIB. Therefore, the first step was to perform gradient field denoising by using the FMRIB [20] plug-in on EEGLAB. The algorithm used by the FMRIB plug-in is the FASTER algorithm [21]. Second, the bandpass filtering method was used for filtering, with a range of 0.01~40 Hz, and the 50 Hz

power frequency interference was filtered out at the same time. Then, referring to the "TREV" scanning mark in the experimental acquisition process, the EEG data was segmented, and the baseline was corrected. Finally, an ICA was used to detect the noise component, and the EEGLAB plug-in EEG Independent Component Labeling was used to assist in identifying and removing interference components such as eye movement and head movement.

In this paper, the DPARSF [22] toolbox in MATLAB was used to preprocess the fMRI data. First, the fMRI data were converted from the Digital Imaging and Communications in Medicine (DICOM) format to the Neuroimaging Information Technology Initiative (NIFTI) format. Then, the fMRI images were slice-time layer corrected, head motion corrected, and normalized to the Montreal Neurological Institute (MNI) space with a voxel size of 3 × 3 × 3 mm^3. Next, a Gaussian kernel with a full-width at half maximum (FWHW) of 4 × 4 × 4 mm^3 was used for spatial smoothing to improve the signal-to-noise ratio. Finally, a bandpass filter with a cutoff frequency of 0.01~0.08 Hz was used for filtering. It should be noted that the fMRI data with a head motion amplitude greater than 2 mm horizontal motion or 2° rotation angle are considered to have poor data quality and should be eliminated.

2.4. Empirical mode diagram decomposition

The empirical mode diagram decomposition (EMDD) is a four-dimensional extension of FATEMD [16]. It adds a time variable to the original three-dimensional volume decomposition, that is, it optimizes the number of iterations under specific time conditions and can be used for the decomposition and analysis of the fMRI data. The steps of using the EMDD method to decompose a four-dimensional data $K(x, y, z, t)$ are as follows:

1) Set $i = 1$, $R_i(x, y, z, t) = K(x, y, z, t)$.

2) A 4D window of size $4 \times 4 \times 4 \times 4$ is used to determine the local maxima and minima that are strictly above (or below) all neighboring values contained in the four-dimensional data.

3) Calculate the size of the maximum and minimum filters that will be used to make the extreme envelope and its smoothing. The maximum and minimum filters are made by calculating the closest Euclidean distance between the maximum point $d_{k.max}$ and the minimum point $d_{k.min}$. Then, determine the window width w_{en} of the maximum and minimum filters using the formula $w_{en} = min\{min\{d_{k.max}\}, min\{d_{k.min}\}\}$.

4) Create a maximum envelope $Env_{max}(x, y, z, t)$ and a minimum envelope $Env_{min}(x, y, z, t)$ of size w_{en}.

5) Compute the smoothed envelope using a mean filter: $Env_{max-s}(x, y, z, t)$ and $Env_{min-s}(x, y, z, t)$.

6) The mean filter $Env_A(x, y, z, t)$ is calculated by averaging the smoothed upper and lower envelopes.

7) Calculate the i-th SIMF: $SIMF_i(x, y, z, t) = R_i(x, y, z, t) - Env_A(x, y, z, t)$.

8) Calculate $R_{i+1}(x, y, z, t) = R_i(x, y, z, t) - \sum_{i=1}^{i} SIMF_i(x, y, z, t)$.

9) If $R_{i+1}(x, y, z, t)$ contains more than two extreme values, then go to step 2) and set $i = i + 1$; otherwise, the EMDD decomposition is completed. In general, the four-dimensional data $K(x, y, z, t)$ can be reconstructed based on the sum of n SIMFs and residuals as follows:

$$K(x, y, z, t) = \sum_{t=1}^{T} \left[\sum_{i=1}^{n} SIMF_i(x, y, z, t) + R_{n+1}(x, y, z, t)\right]. \quad (1)$$

This study designed the EMDD algorithm to decompose the fMRI image within an fMRI scan time and to extract its high-frequency component SIMF as the spatial prior for EEG source localization, as shown in the following formula (2):

$$fMRI(x, y, z, t) = \sum_{t=1}^{T} [\sum_{i=1}^{n} SIMF_i(x, y, z, t) + residue(x, y, z, t)]. \quad (2)$$

Among them, $SIMF_1$ contains the highest frequency voxels in the fMRI activation map, $SIMF_2 \sim SIMF_n$ is the spatial activation map with increasingly lower frequencies, and residue represents the intensity trend of the voxel in the original fMRI map.

The pseudocode of the EMDD algorithm is as follows:

```
function [SIMF, Residual, Reconstructed] = EMDD (K)
    [x, y, z, t] = size (K); % Dimensions of input data
    R = K; % Initialize residual R_i
    i = 1; % SIMF index
    SIMF = []; % Store SIMFs
    threshold = 2; % Minimum number of extrema to continue
    max_iter = 100; % Limit maximum iterations to prevent infinite loops
    while true
        % Step 1: Identify extrema using a 4D window of size 4 × 4 × 4 × 4
        LocalMax = islocalmax (R, [1 2 3 4]); % Find local maxima
        LocalMin = islocalmin (R, [1 2 3 4]); % Find local minima
        % Step 2: Calculate distances between extrema
        [MaxPos, MinPos] = findExtremaPositions (LocalMax, LocalMin, R);
        d_max = calculateDistances (MaxPos); % Distances between maxima
        d_min = calculateDistances (MinPos); % Distances between minima
        % Step 3: Calculate window width for envelopes
        w_en = min([min(d_max), min(d_min)]);
        % Step 4: Create maximum and minimum envelopes
        Env_max = createEnvelope (R, MaxPos, w_en);
        Env_min = createEnvelope (R, MinPos, w_en);
        % Step 5: Smooth the envelopes using a mean filter
        Env_max_s = smoothEnvelope (Env_max);
        Env_min_s = smoothEnvelope (Env_min);
        % Step 6: Compute the mean envelope
        Env_A = (Env_max_s + Env_min_s) / 2;
        % Step 7: Calculate the i-th SIMF
        SIMF_i = R - Env_A;
        SIMF(:, :, :, :, i) = SIMF_i; % Store the SIMF
        % Step 8: Update the residual
        R = R - SIMF_i;
        % Check stopping criteria
        if countExtrema(R) <= threshold || i >= max_iter
            break;
        end
        % Update SIMF index
```

```
        i = i + 1;
    end
    % Final residual
    Residual = R;
    % Step 9: Reconstruct the original data
    Reconstructed = sum (SIMF, 5) + Residual;
end
```

2.5. Extraction of fMRI functional networks

The preprocessed fMRI functional images were subjected to ICA by the Group ICA of fMRI Toolbox (GIFT) to obtain several spatial independent components. Each spatial independent component was Z-transformed, and voxels with Z scores greater than 3 were set as activated voxels. Then, the spatial multiple linear regression algorithm was used to sort each independent component to find the independent component that matched the resting state network, so as to use it as a priori constraint for EEG source imaging. Related studies [4,23,24] have found that the default mode network with cognitive control, emotion regulation, and memory inhibition was significantly different between the IBD patients and the healthy controls; CD patients had a reduced functional connectivity in the cerebellum and postcentral gyrus in the salience network, and the salience network is related to emotional stimulation and pain processing. These changes may be related to emotional regulation disorders and impaired sensory stimulation processing in IBD patients. IBD patients have a decreased verbal IQ and language learning ability in the absence of disease activity characteristics, which may provide a neurophysiological basis for language disorders in IBD patients. Therefore, this study focused on extracting the default mode network, salience network, and language network, and constructed a spatial covariance basis as a priori constraints.

2.6. Establishment of forward head model

The head model is a computational model of the EEG forward problem, which determines the impact level of a given neural current source in the brain on each electrode on the scalp and provides a guiding field matrix to solve the inverse problem. At present, the mainstream method to construct a head model is the boundary element model (BEM) in a real head model. The boundary element model uses triangular meshes to simulate the interface between each tissue in the head, such as the air/scalp, scalp/skull, and skull/brain interfaces. Each type of tissue is considered to be electrically uniform and isotropic, and each tissue has a different conductivity value. In this study, the head model mesh was first constructed using the brain structure data of the subjects, and the electrode distribution coordinates were aligned with the cortical mesh. Then, the typical mesh in the brain template was spatially transformed to generate a BEM three-layer real head model, thereby calculating the guiding field matrix.

2.7. Parametric empirical Bayesian inverse modeling

The parametric empirical Bayesian model [25,26] is used for EEG source imaging:

$$\begin{matrix} Y = LS + \varepsilon_1 \quad \varepsilon_1 \sim N(0, T, C_1) \\ S = 0 + \varepsilon_2 \quad \varepsilon_2 \sim N(0, T, C_2) \end{matrix}, \tag{3}$$

where $Y \in R^{n\times m}$ is the EEG recording signal with n electrodes and m sampling points. $L \in R^{n\times d}$ is the guidance field matrix calculated by the forward model, which reflects the mapping relationship between the brain sources and sensors. $S \in R^{d\times m}$ is the unknown source of d dipoles. ε_1 and ε_2 represent random fluctuations in sensor space and source space, respectively. $N(\mu, T, C)$ represents the multivariate Gaussian distribution of ε with a mean μ and a covariance $T \otimes C$, $\otimes$ represents the Kronecker tensor product, and T represents time. In the sensor space, we assume $C_1 = \alpha^{-1} I_n$ to encode the covariance of the sensor noise, where I_n is the n-dimensional identity matrix. In the source space, we express it in the following form of covariance components:

$$C_2 = \sum_{i=1}^{k} \lambda_i V_i, \tag{4}$$

where $\lambda = [\lambda_1, \lambda_2, \ldots, \lambda_k]^T$ is a k-dimensional non-negative hyperparameter vector that represents the weight coefficients of each covariance matrix V_i. The hyperparameters λ are unknown, and they are similar to the standard regularization parameters in ill-posed problems. These hyperparameters can be estimated using the maximum restricted likelihood algorithm (ReML), which simultaneously generates a maximum a posteriori estimate of the source distribution [27].

In the Bayesian framework, the logarithmic model evidence $\ln p(Y \mid \lambda)$ is the restricted likelihood function of the observed variables, and the brain power S is estimated by maximizing the posterior probability, which can be approximated by maximizing the free energy F [28]. The free energy F is related to the model evidence and is the lower limit of the model evidence. The calculation formula of the free energy [29] is as follows:

$$F = -\frac{1}{2} tr(G^{-1} Y Y^T) - \frac{1}{2} \ln |G| - \frac{1}{2} (\alpha - \eta)^T \Omega^{-1} (\alpha - \eta) + \frac{1}{2} ln|\Sigma \Omega^{-1}|, \tag{5}$$

where $G = LC_2L^T + C_1$. The first two terms in formula (4) represent the degree of fit of the Bayesian posterior probability to the model, and the last two terms represent the regularization term or penalty term of the model complexity. We need to find a balance between the fit and complexity and make the model complexity moderate by summing the parameters in the marginalized model. The larger the Bayesian log-model evidence, the better the model performance and the more accurate the estimated source distribution. Once the maximum log-model evidence is determined, the unknown source S can be calculated as follows:

$$S = max_S P(S \mid Y) = MY. \tag{6}$$

$M = C_2 L^T G^{-1}$ is the inverse operator based on the optimal expected value of the hyperparameters.

2.8. Effective connectivity analysis

The effective connectivity refers to the causal relationship between different brain regions, that is, how the activity of one region affects the activity of another region [30]. This connectivity takes the specific path and direction of the signal transmission into account, thus reflecting how information is transmitted and executed in the brain. Due to the influence of the volume conduction on the sensitivity of the EEG source analysis [31], when analyzing the brain network connectivity, one study [32] found that mapping EEG signals recorded from the scalp to the corresponding areas of the cerebral cortex through source reconstruction technology could generate cortical source activity signals with a higher temporal resolution, which significantly reduced the problems caused by volume conduction effects

and improved the accuracy of the brain neural network connectivity analysis.

Phase transfer entropy (PTE) [33] specifically analyzes the directional information exchange between the time series and quantifies the amount of information transferred by evaluating the change in the entropy of information flow between different time series. When volume conduction exists, PTE helps to find deviations in the information transfer and identify whether there is a true causal relationship between the signals [34]. PTE has no specific upper limit, so directional phase transfer entropy (dPTE) [35] is used to standardize the PTE:

$$dPTE_{x\to y} = \frac{PTE_{x\to y}}{PTE_{x\to y}+PTE_{y\to x}} \tag{7}$$

The value range of $dPTE_{x\to y}$ is 0~1. When $dPTE_{x\to y} > 0.5$, the signal preferentially flows from X to Y, and when $dPTE_{x\to y} < 0.5$, the signal flows from Y to X. When $dPTE_{x\to y}$ is about 0.5, it means that the information flow between the two signals is relatively balanced and has no obvious directionality.

In this paper, we used the time series of EEG data recorded by 64 electrode leads to calculate its dPTE, analyze the effective connectivity between various possible combinations of cortical source activities, and reveal the directionality of information transmission between brain regions. Furthermore, it can be verified that the abnormal brain sources of IBD obtained by EMDD-based EEG-fMRI source imaging are indeed different from those of the healthy group. We further subdivided the distribution of dipoles into 68 specific brain regions (Regions pf Interest, ROI) based on the Desikan-Killiany brain anatomical template [36]. For each ROI in the template, we calculated the average value of the current source density of all voxels in it and generated the time series data corresponding to each region. Then, the time series corresponding to each ROI was cut into 2 s time windows, and the dPTE values of these windows were calculated and averaged. To determine whether there is a clear directional connectivity between two ROIs, we used a nonparametric test method to permutate the information flow dataset composed of all dPTE values to control the family-wise error rate (FWER). To understand how brain source activity exhibits unique characteristics in different regions at a macro level, we further classified the 68 ROIs into 14 different brain regions according to their anatomical locations in the Desikan-Killiany template, including the left prefrontal lobe (LPF), right prefrontal lobe (RPF), left frontal lobe (LF), right frontal lobe (RF), left central lobe (LC), right central lobe (RC), left parietal lobe (LP), right parietal lobe (RP), left occipital lobe (LO), right occipital lobe (RO), left temporal lobe (LT), right temporal lobe (RT), left limbic system (LL), and right limbic system (RL). Then, we performed a permutation test on the average information flows of the IBD group and the healthy group, and screened out the directional information flows with significant differences ($p < 0.05$) to construct a brain network connectivity map.

3. Results

In order to make full use of the complementary information of EEG and fMRI signals in terms of the temporal and spatial resolution, we used a new multimodal integrated source imaging method to provide an accurate source reconstruction of cortical activity. At the same time, it compared the EEG source imaging based on fMRI spatial constraints, and then performed an effective connectivity analysis on the reconstructed cortical activity time series.

3.1. Source imaging results

As shown in Table 1, the first column is the EEG source imaging brain area results based on fMRI functional network constraints, and the second column is the EEG-fMRI source imaging results based on EMDD. They were compared with the results of existing literature studies [3,4,23,24] and we found that the two methods accurately located the abnormal brain areas of IBD. In the EEG-fMRI source imaging based on EMDD, abnormal brain areas that did not appear in previous studies were also obtained: Uncus, Claustrum, Lenticular nucleus, and Lingual gyrus. The uncus is the front structure of the parahippocampal gyrus of the brain, and the lingual gyrus is part of the medial occipitotemporal gyrus. Strictly speaking, both of them belong to the range of abnormal brain areas found in existing studies; however, through the method of this study, they can be accurately located, thereby improving the accuracy of the source imaging. A schematic diagram of brain areas obtained by EEG-fMRI source imaging based on EMDD is shown in Figure 2 below.

Table 1. Abnormal brain regions in IBD patients.

fMRI informed EEG source imaging	$SIMF_1$ informed EEG source imaging	Abnormal brain regions in IBD from existing literature [3,4,23,24]
Inferior temporal gyrus	Inferior temporal gyrus	Inferior temporal gyrus
Middle temporal gyrus	Middle temporal gyrus	Middle temporal gyrus
Superior temporal gyrus	Superior temporal gyrus	Superior temporal gyrus
Transverse temporal gyrus	Transverse temporal gyrus	Transverse temporal gyrus
Fusiform gyrus	Fusiform gyrus	Fusiform gyrus
Parahippocampal gyrus	Parahippocampal gyrus	Hippocampus
Superior frontal gyrus	Superior frontal gyrus	Parahippocampal gyrus
Middle frontal gyrus	Middle frontal gyrus	Superior frontal gyrus
Inferior frontal gyrus	Inferior frontal gyrus	Middle frontal gyrus
Inferior parietal lobule	Inferior parietal lobule	Inferior parietal lobule
Posterior cingulate gyrus	Posterior cingulate gyrus	Superior parietal lobule
Insula	Insula	Anterior cingulate cortex
Amygdala	Thalamus	Posterior cingulate cortex
Precentral gyrus	Amygdala	Insula
Postcentral gyrus	Precentral gyrus	Thalamus
	Postcentral gyrus	Amygdala
	Uncus	Caudate nucleus
	Claustrum	Precentral gyrus
	Lentiform nucleus	Postcentral gyrus
	Lingual gyrus	Cerebellum

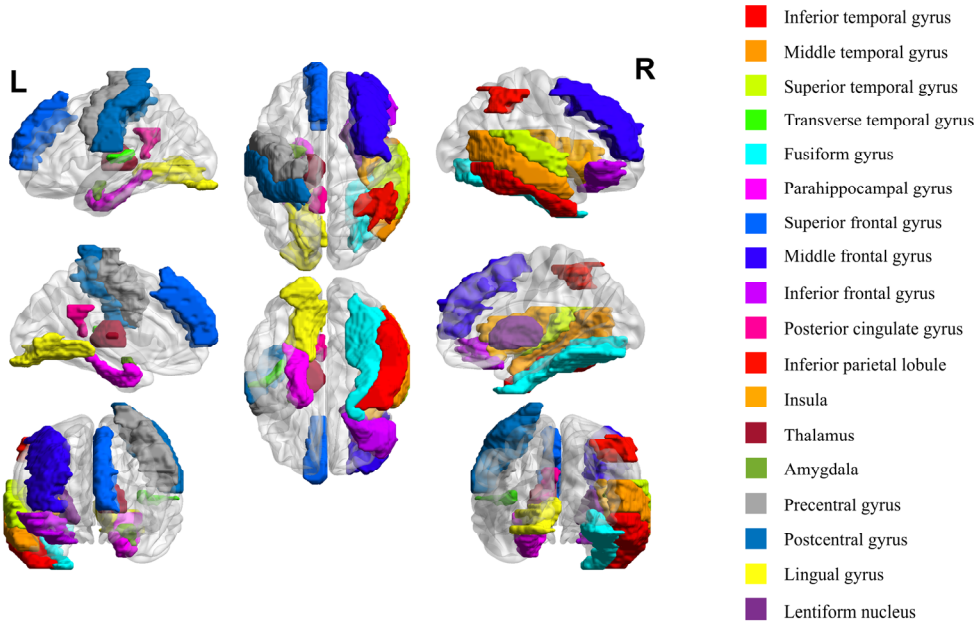

Figure 2. Schematic diagram of brain regions obtained from EEG-fMRI source imaging based on EMDD.

Figure 3 shows the results of two source imaging methods. Compared with (a), (b) shows that the areas with originally high activation intensity have become sparsely concentrated, many "pseudo sources" have disappeared, and the activation intensity threshold is also higher.

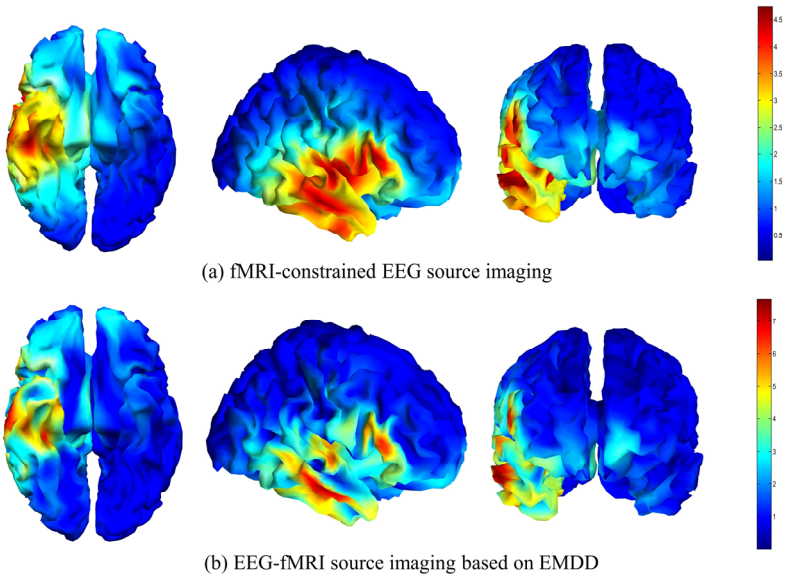

Figure 3. fMRI-constrained EEG source imaging (a) and EEG-fMRI source imaging based on EMDD (b) in the same IBD patient. It is displayed from the coronal, sagittal, and axial positions in turn. The jet color bar on the right represents the activation intensity. The maximum activation value in (a) is 4.7, and the maximum activation value in (b) is 7.5.

At the same time, the two methods were applied to healthy subjects, and the source imaging results showed that the whole brain activation intensity was in a weak state, which was related to the resting state acquisition method of the subjects. As shown in Figure 4, the red part represents the brain area with a stronger activation intensity, and the blue part represents the brain area with a weaker activation intensity, though their activation thresholds are all lower than the abnormal brain area activation intensity of IBD patients. A study [37] showed that there are functional activities in the brain at rest and these activities may be organized. The brain areas that produce activities mainly include the medial prefrontal lobe, the anterior cingulate gyrus, the posterior cingulate gyrus, and the inferior parietal lobules on both sides. As shown in Figure 4, the EEG source imaging using the EMDD algorithm to extract fMRI high-frequency components as constraints shows a clearer and more specific relatively high-activated brain area, which is consistent with the characteristics of the resting brain activity network in previous studies.

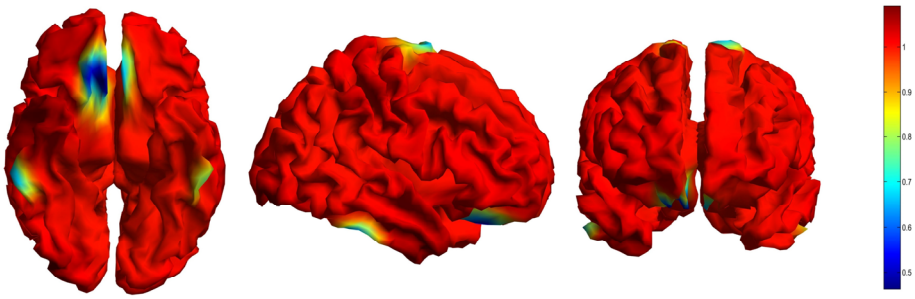

(a) fMRI-constrained EEG source imaging

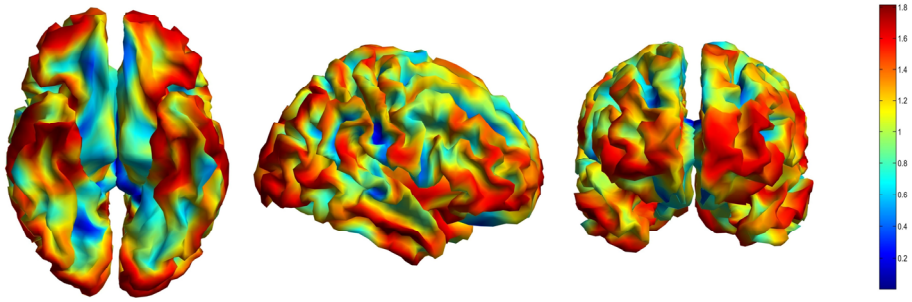

(b) EEG-fMRI source imaging based on EMDD

Figure 4. fMRI-constrained EEG source imaging (a) and EEG-fMRI source imaging based on EMDD (b) in the healthy subject. It is displayed from the coronal, sagittal, and axial positions in turn. The jet color bar on the right represents the activation intensity. The maximum activation value in (a) is 1.1, and the maximum activation value in (b) is 1.8.

3.2. Performance comparison of two source imaging methods

In this paper, log model evidence (LME) and explained variance (EV) [38] were used to compare the performance of two source imaging methods. LME is defined as the logarithm of the marginal likelihood and is approximated by the free energy. This metric is used to assess the relative usefulness of different models, and models with a higher LME are usually selected because it provides a balance between the model complexity and accuracy. EV represents the proportion of the data that fits across all sensors and time intervals and is used to assess the source imaging model's ability to explain the

data. A higher EV means that the model is able to capture the variability in the data well (i.e., the model is able to explain most of the observed data).

As shown in Figure 5, the LME of the IBD group was compared using the two source imaging methods. The LME obtained from all patients in the IBD group was visualized, and it was found that the LME obtained by EEG-fMRI source imaging based on EMDD was generally higher than that obtained by EEG source imaging based on fMRI constraints.

Table 2 shows the average LME of the IBD group and the healthy group under the two source imaging methods. In the IBD group, the average LME obtained by EEG-fMRI source imaging based on EMDD was 5451, and the average LME obtained by EEG source imaging based on fMRI constraints was 4206; the former was 29.60% higher than the latter. In the healthy group, the average LME obtained by EEG-fMRI source imaging based on EMDD was 41.50% higher than that obtained by EEG source imaging based on fMRI.

In Figure 6, the EV of the IBD group by the two source imaging methods was compared. As can be seen from the figure, the EV obtained by EEG-fMRI source imaging based on EMDD is generally higher than that obtained by EEG source imaging based on fMRI constraints, with the highest value reaching 92.71%. There are great differences in the EV of different subjects in the same group, with individual differences being a major factor. There are innate differences between different subjects, including the brain anatomical structure, functional organization, and neural activity patterns, which lead to differences in spatial distribution, pattern, and intensity of source activity.

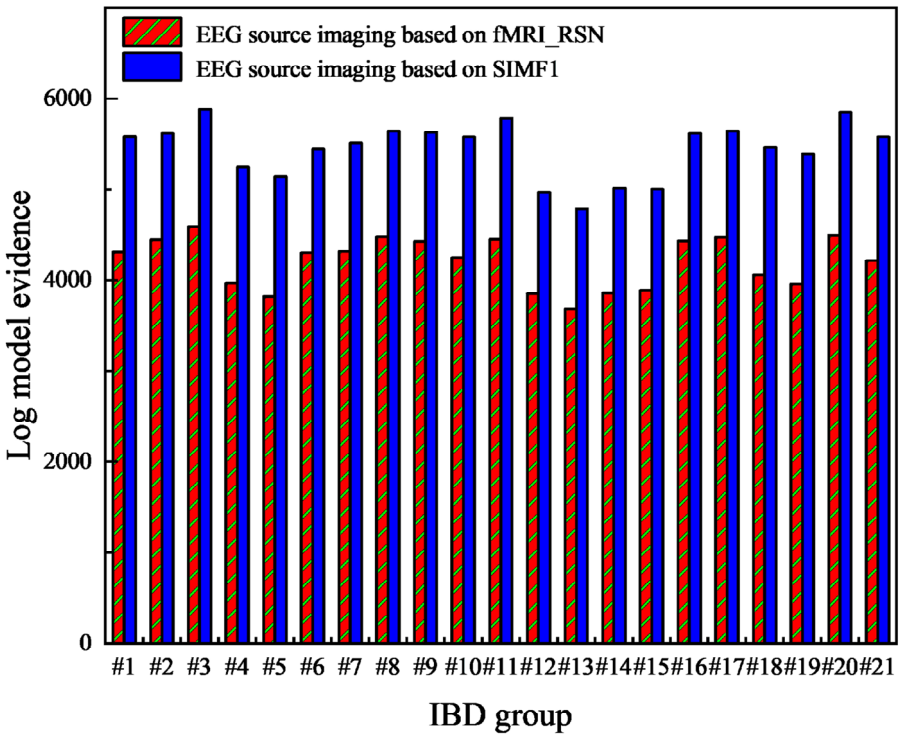

Figure 5. Histogram of LME obtained by two source imaging methods. The horizontal axis represents 21 IBD subjects. The red striped columns represent the LME of EEG source imaging based on fMRI constraints, and the blue columns represent the LME of EEG-fMRI source imaging based on EMDD.

Table 2. Statistical results of log model evidence (mean ± standard deviation).

Log model evidence	fMRI + EEG	$SIMF_1$ + EEG	Average improvement (%)
IBD group	4206 ± 279	5451 ± 307	29.60
Healthy group	4236 ± 379	5994 ± 367	41.50

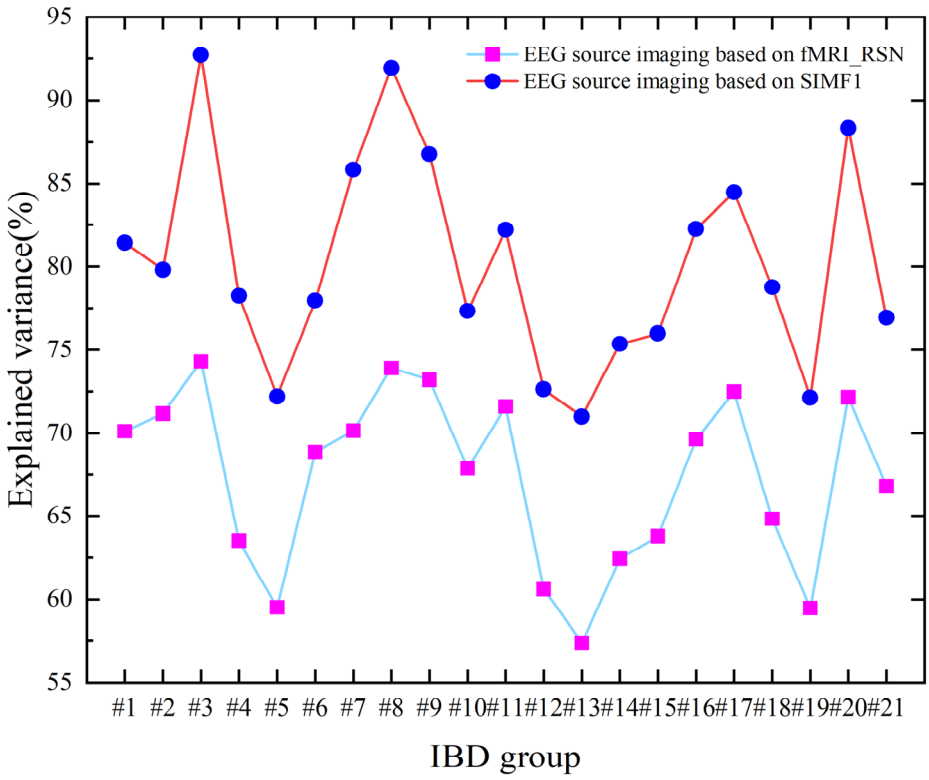

Figure 6. Line graph of EV by two source imaging methods. The horizontal axis represents 21 IBD subjects. The pink block nodes represent the EV of EEG source imaging based on fMRI constraints, and the blue nodes represent the EV of EEG-fMRI source imaging based on EMDD.

Table 3. Statistical results of explained variance (mean ± standard deviation).

Explained variance	fMRI + EEG	$SIMF_1$ + EEG	Average improvement (%)
IBD group	67.32 ± 5.27	80.19 ± 6.35	19.12
Healthy group	66.68 ± 4.89	78.91 ± 4.58	18.34

Table 3 shows the average EV of the IBD group and the healthy group under the two source imaging methods, as well as the improvement level of EV between EEG-fMRI source imaging based on EMDD and EEG source imaging based on fMRI. In the IBD group, the average EV obtained by EEG-fMRI source imaging based on EMDD was improved by 19.12% compared with that obtained by EEG source imaging based on fMRI. In the healthy group, the average EV obtained by EEG-fMRI source imaging based on EMDD was improved by 18.34% compared with that obtained by EEG source imaging based on fMRI. Under the same source imaging method, the EV obtained by the IBD

group and the healthy group was slightly different, which was within the normal range.

3.3. Effective connectivity analysis

PTE was used in the effective connectivity analysis of the reconstructed cortical source time series, and it was standardized as the directional phase transfer entropy (dPTE) to identify the directional connectivity between ROIs. As shown in Figure 7, (a) is the PTE information flow of the healthy group, and (b) is the PTE information flow of the IBD group. Both are dPTE value matrices. In order to obtain a clear directional information flow, (a) and (b) were thresholded to obtain the significant PTE information flow of the healthy group (c) and the significant PTE information flow of the IBD group (d). It is not difficult to see that the number of significant information flows in the healthy group is greater than that in the IBD group. The IBD group mainly lacked information flows in the frontal lobe, temporal lobe, and parietal lobe, while significant information flows appeared in the superior temporal gyrus and transverse temporal gyrus, which was different from the healthy control group.

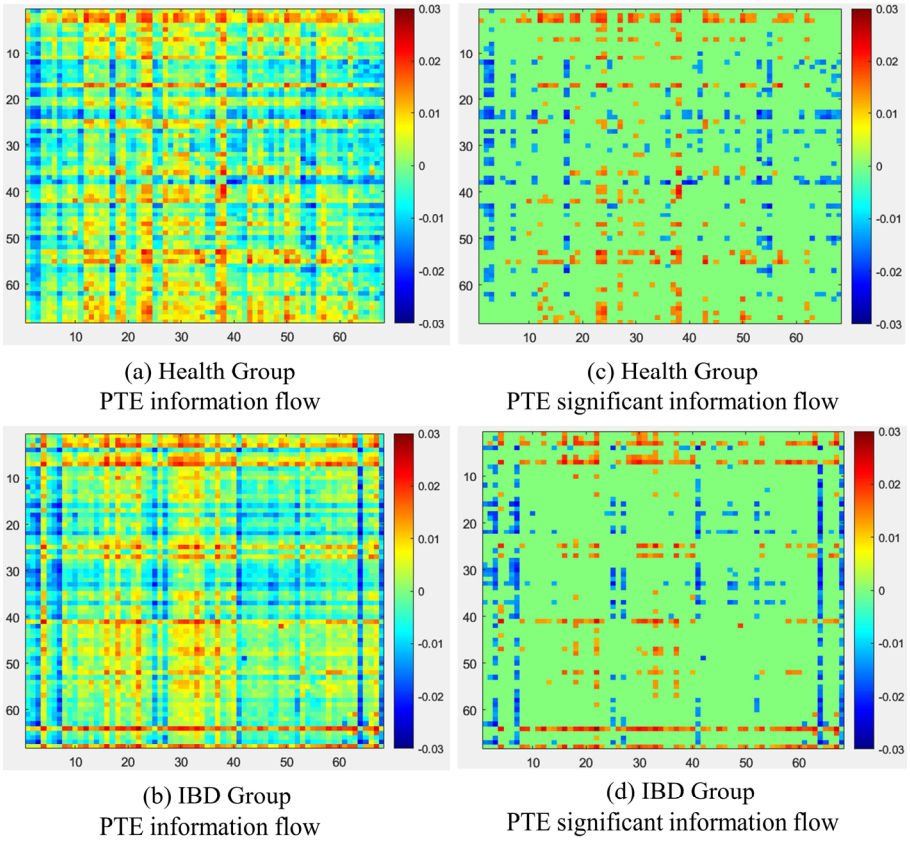

Figure 7. Comparison of information flow between the healthy group and the IBD group. (a) is the PTE information flow of the healthy group, and after thresholding, the significant PTE information flow (c) is obtained. (b) is the PTE information flow of the IBD group, and after thresholding, the significant PTE information flow (d) is obtained. The red blocks indicate that information flows from the brain area corresponding to the row to the brain area corresponding to the column, while the blue blocks indicate the opposite.

The effective connectivity diagrams of the brain networks of the IBD group and the healthy group are shown in Figures 8 and 9, respectively. The blue and pink connectivity lines indicate the different directions of information flow. Overall, the IBD group had information flow loss in the left and right frontal lobes, the left and right central regions, the left parietal lobe, and the right temporal lobe. Specifically, the IBD group had information flow loss in the superior frontal gyrus, middle frontal gyrus, inferior frontal gyrus, paracentral lobule, fusiform gyrus of the left and right hemispheres, the precentral gyrus, inferior parietal gyrus, lateral occipital lobe, insula of the right hemisphere, and the superior parietal gyrus, precuneus, and anterior cingulate gyrus of the left hemisphere. Compared with the effective connectivity of the brain network of the healthy group, the information flow intensity of the left parahippocampal gyrus of the IBD group was enhanced, the information flow intensity of the right parahippocampal gyrus was weakened, and the information flow intensity of the right lingual gyrus was also enhanced.

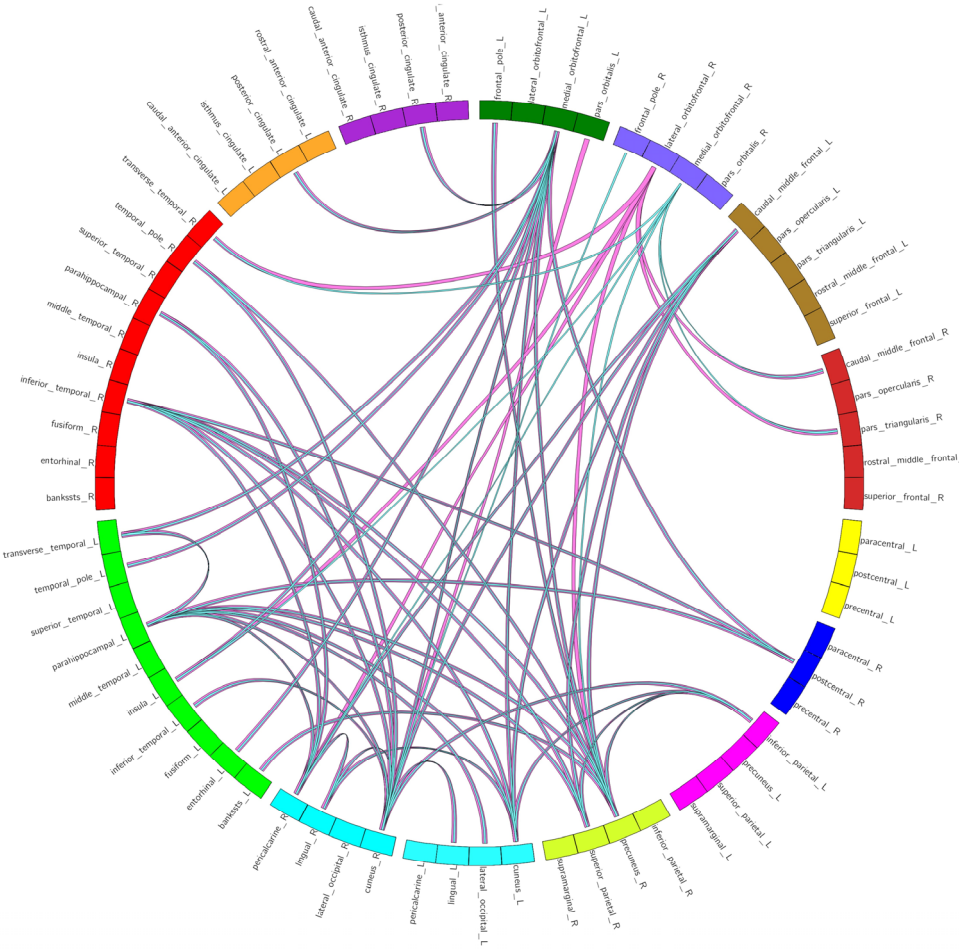

Figure 8. Brain network effective connectivity map of IBD group. The 68 brain regions of the Desikan-Killiany template are classified into 14 different brain regions. Light blue and pink lines indicate opposite information flows.

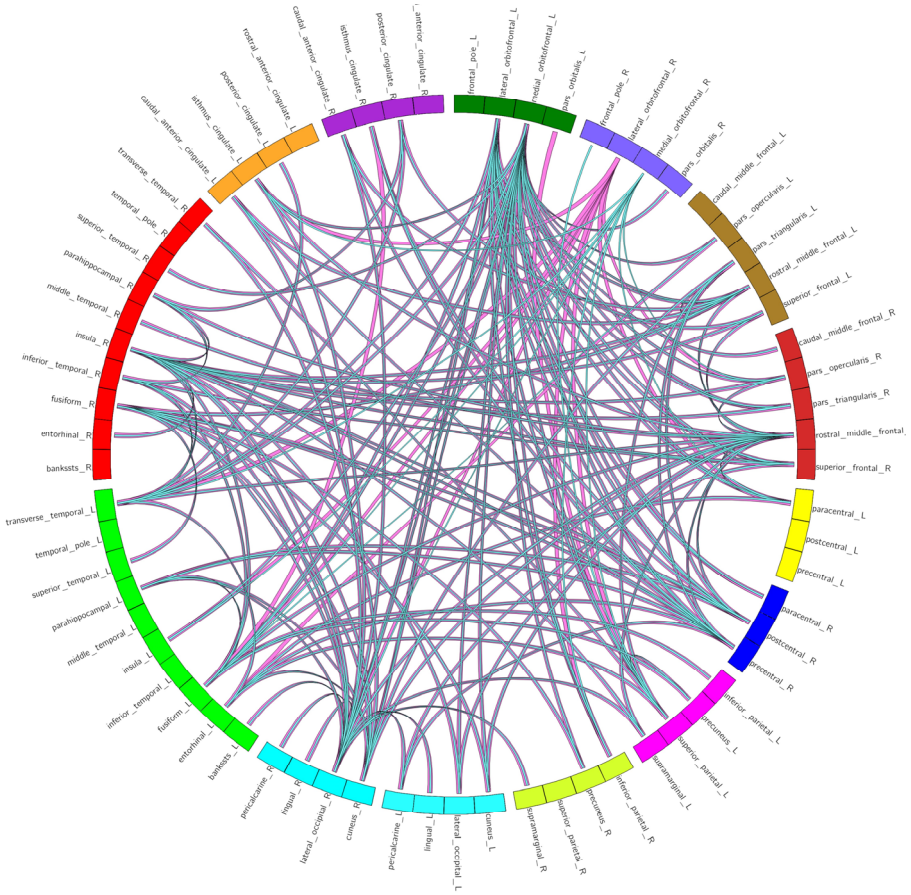

Figure 9. Brain network effective connectivity map of the healthy group. The 68 brain regions of the Desikan-Killiany template are classified into 14 different brain regions. Light blue and pink lines indicate opposite information flows.

4. Discussion

In the research on the brain of IBD patients, magnetic resonance imaging technology is currently the mainstream direction. However, most studies only focus on single-modality imaging data, which limits the research on the brain function and structure, which lacks comprehensiveness. In this study, we used the complementary information of EEG and fMRI signals in terms of the spatiotemporal resolution to propose a new EEG-fMRI source imaging method, namely a spatiotemporal constrained EEG-fMRI source imaging method based on empirical mode graph decomposition, which accurately found the location of abnormal sources in the brain of IBD patients, reconstructed the traceability time series from the cortical source for an effective connectivity analysis, and studied the directional connectivity of the brain network of IBD patients, thereby providing a theoretical basis to explore new indicators for clinical diagnoses and treatments.

EEG is a highly underdetermined inverse problem with infinite solutions [39], so it often produces overly blurred and diffuse source estimates. Prior information is needed to constrain the solution space to obtain a unique solution. Parametric Empirical Bayesian (PEB) introduces fMRI information as a prior constraint and measures its relative weight through hyperparameters determined by EEG data. The introduction of Network based on Source Imaging (NESOI) [40] provides a practical method to

fuse the resting-state fMRI data with EEG as a prior constraint. Specifically, this method uses an ICA to extract the brain functional networks in fMRI data and construct covariance priors. However, most EEG methods cannot locate deep brain sources. Due to the volume conduction effect of the head, the recorded potentials are generally associated with low-intensity dipoles on the surface of the brain, rather than with high-intensity sources in deep brain regions such as the insula and thalamus. The EMDD proposed in this paper can decompose the fMRI data in the time series into a series of SIMFs of different frequencies. The first extracted high spatial frequency SIMF had more mutations, peaks, and underestimation, so $SIMF_1$ had rich spatial details. The ICA was performed on $SIMF_1$ to obtain the resting state functional network (default mode network, salience network, and language network) and to construct covariance prior.

We compared the performance of two methods, EEG-fMRI source imaging based on EMDD and EEG source imaging based on fMRI constraints, and reconstructed the time series from cortical source space for an effective connectivity analysis. The results showed that using $SIMF_1$ as a priori constraint can improve the accuracy of EEG source imaging and make the localization of brain sources sparser, that is, the location and size of the reconstructed sources are more accurate. Compared with the results of existing literature studies, the two source imaging methods accurately located abnormal brain regions in IBD, and in the EEG-fMRI source imaging method based on EMDD, abnormal brain regions that did not appear in previous studies were also obtained: Uncus, Claustrum, Lentiform nucleus and Lingual gyrus. The uncus is the anterior structure of the parahippocampal gyrus of the brain and is part of the limbic system. It is very close to the anatomical position of the amygdala and is involved in olfaction, emotional memory, and fear response. It plays an indirect role in emotional processing [41]. Its abnormalities may be related to the anxious behavior of IBD patients, especially intestinal inflammation, which activates the limbic system through the vagus nerve or circulating inflammatory factors (such as IL-6, TNF-α), thus leading to imbalance in emotional regulation. The claustrum is located deep in the insula and has direct connections to almost all brain areas of the cerebral cortex. It is a connection center in the brain and is considered to be the "switch" that integrates perception and consciousness. It integrates sensory information and regulates the formation and maintenance of consciousness in various ways. It plays an important role in sensory information processing and cognitive function regulation [42]. Its abnormality may be related to the central processing disorder of visceral pain signals in IBD patients or affect the perception of chronic inflammation through the gut-brain axis. Animal models [43] have shown that anxiety-like behavior in mice with chronic colitis is associated with changes in activity in atypical brain regions (such as the claustrum) outside the hippocampus and prefrontal cortex, thus supporting the potential role of the newly discovered brain region. The lenticular nucleus belongs to the basal ganglia, which is composed of the putamen and the globus pallidus. It is located deep in the insula and lateral to the thalamus. It is involved in emotion regulation, especially emotions related to rewards and social behavior. It participates in higher cognitive functions such as decision making, working memory, and attention control through connectivity with the prefrontal cortex. The lenticular nucleus is also a key area for motor control. It affects fine motor skills by regulating muscle tension and coordinating movements [44]. Abnormal activities in the lentiform nucleus may reflect motor inhibition or depressed moods caused by chronic pain or fatigue in IBD patients. The lingual gyrus is part of the medial occipitotemporal gyrus and is mainly involved in visual information processing, though its connection with the DMN may indirectly affects the patient's attention allocation to disease symptoms and the amplification of negative emotions. Studies have shown that abnormalities or damage to the lingual gyrus are associated with

anxiety and depression [45]. It can be seen that EEG-fMRI source imaging based on empirical mode graph decomposition has a significant effect on the localization of deep brain regions and can obtain more sparse and concentrated sources.

After analyzing the effective connectivity of the cortical source brain network in the IBD group and the healthy group, it was found that the connectivity density of the cortical source brain network in the healthy group was high, and the bidirectional information flow between brain regions was significant, while the IBD group had information flow loss in the left and right frontal lobes, the left and right central areas, the left parietal lobe, and the right temporal lobe. The information flow intensity of the left parahippocampal gyrus was enhanced, while the information flow intensity of the right parahippocampal gyrus was weakened. The information flow intensity of the right lingual gyrus was also enhanced, specifically, the right lingual gyrus of the healthy group was only bidirectionally connected to the lateral side of the right occipital lobe, while the right lingual gyrus of the IBD group was bidirectionally connected to the cuneus of the left and right hemispheres and the right paracalcarine gyrus. The cuneus and paracalcarine gyrus are both located in the occipital lobe. Structurally, the paracalcarine gyrus divides the visual cortex into two, separating the upper cuneus and the lower lingual gyrus [46]. The cuneus, paracalcarine gyrus, and lingual gyrus are all related to visual memory and logical analysis [47]. An abnormal or damaged lingual gyrus may be related to visual snow and aphasia, as well as anxiety and depression [48,49]. Therefore, the enhanced bidirectional connectivity between the lingual gyrus and the cuneus and paracalcarine gyrus in IBD patients may be one of the intrinsic reasons for anxiety, depression, and other emotional disorders in IBD patients. These brain regions with abnormal inflow, outflow, or loss of information flow also confirm the results of the previous source imaging.

In addition, there are still some limitations in this study. First, inflammatory bowel disease has different subtypes, mainly including Crohn's disease and ulcerative colitis, and different disease states, which are divided into active phase and remission phase. Due to the difficulty of EEG-fMRI synchronous acquisition experiments and the small number of recruited patients, this paper did not subdivide the disease types or disease states, but only analyzed the brain structure and function of IBD patients in general. Therefore, the research results are not precise. In future work, more IBD patients can be recruited and subdivided, so as to conduct a deeper study on the brain structure and function of different subtypes and disease states of IBD, and provide a new perspective for personalized clinical medicine. Second, the stability and robustness of the EEG-fMRI source imaging method based on empirical mode graph decomposition proposed in this paper need to be further explored.

5. Conclusions

This paper proposed an EEG-fMRI source imaging method based on EMDD and reconstructed cortical source signals for an effective connectivity analysis, thereby aiming to explore abnormal brain areas in IBD patients and evaluate the connectivity accuracy of cortical brain networks. The results showed that the EMDD-based EEG-fMRI source imaging method had a better performance. We discovered abnormal brain areas in IBD that were not mentioned in previous studies: the uncus, claustrum, lentiform nucleus, and lingual gyrus. In addition, from the effective connectivity analysis of cortical source signals, we found that IBD patients had an information flow loss in the frontal lobes, central areas, left parietal lobe, and right temporal lobe, and the information flow intensity of the right lingual gyrus was enhanced. The method proposed in this paper makes it possible to detect the source

activity in deep brain areas and provides a theoretical basis to explore new indicators for clinical diagnoses and treatments.

Use of AI tools declaration

The authors declare they have not used Artificial Intelligence (AI) tools in the creation of this article.

Ethics approval of research

The study was conducted in accordance with the Declaration of Helsinki, and approved by Changzhou University Biomedical Ethics Committee (protocol code 20240308015). Informed consent was obtained from all subjects involved in the study. Written informed consent has been obtained from the patients to publish this paper.

Acknowledgments

This work was supported by the project of Jiangsu Key Research and Development Plan (BE2021012-2 and BE2021012-5), and Postgraduate Research & Practice Innovation Program of Jiangsu Province (KYCX24_3253).

Conflict of interest

The authors declare there is no conflict of interest.

References

1. T. H. Taft, A. Bedell, M. R. Craven, L. Guadagnoli, S. Quinton, S. B. Hanauer, Initial assessment of post-traumatic stress in a US cohort of inflammatory bowel disease patients, *Inflammatory Bowel Dis.*, **25** (2019), 1577–1585. https://doi.org/10.1093/ibd/izz032
2. T. H. Bisgaard, K. H. Allin, L. Keefer, A. N. Ananthakrishnan, T. Jess, Depression and anxiety in inflammatory bowel disease: epidemiology, mechanisms and treatment, *Nat. Rev. Gastroenterol. Hepatol.*, **19** (2022), 717–726. https://doi.org/10.1038/s41575-022-00634-6
3. A. K. Thomann, M. M. Schmitgen, D. Kmuche, M. P. Ebert, P. A. Thomann, K. Szabo, et al., Exploring joint patterns of brain structure and function in inflammatory bowel diseases using multimodal data fusion, *Neurogastroenterol. Motil.*, **33** (2021), e14078. https://doi.org/10.1111/nmo.14078
4. G. Thapaliya, S. Eldeghaidy, S. J. Radford, S. T. Francis, G. W. Moran, An examination of resting-state functional connectivity in patients with active Crohn's disease, *Front. Neurosci.*, **17** (2023), 1265815. https://doi.org/10.3389/fnins.2023.1265815
5. U. A. Kelleci, T. Calhan, A. Sahin, Z. A. Ozemir, R. Kahraman, K. Ozdil, et al., Electroencephalography findings in Crohn's disease, *Clin. EEG Neurosci.*, **50** (2019), 129–133. https://doi.org/10.1177/1550059418767589

6. A. Kibleur, S. Pellissier, V. Sinniger, J. Robert, E. Gronlier, D. Clarencon, et al., Electroencephalographic correlates of low-frequency vagus nerve stimulation therapy for Crohn's disease, *Clin. Neurophysiol.*, **129** (2018), 1041–1046. https://doi.org/10.1016/j.clinph.2018.02.127
7. Z. Fang, E. Lynn, M. Huc, S. Fogel, V. J. Knott, N. Jaworska, Simultaneous EEG+fMRI study of brain activity during an emotional Stroop task in individuals in remission from depression, *Cortex*, **155** (2022), 237–250. https://doi.org/10.1016/j.cortex.2022.07.010
8. Y. Yang, S. Luo, W. Wang, X. Gao, X. Yao, T. Wu, From bench to bedside: Overview of magnetoencephalography in basic principle, signal processing, source localization and clinical applications, *NeuroImage Clin.*, **42** (2024), 103608. https://doi.org/10.1016/j.nicl.2024.103608
9. K. Yu, X. Niu, B. He, Neuromodulation management of chronic neuropathic pain in the central nervous system, *Adv. Funct. Mater.*, **30** (2020), 1908999. https://doi.org/10.1002/adfm.201908999
10. A. Seeland, M. M. Krell, S. Straube, E. A. Kirchner, Empirical comparison of distributed source localization methods for single-trial detection of movement preparation, *Front. Hum. Neurosci.*, **12** (2018), 340. https://doi.org/10.3389/fnhum.2018.00340
11. R. Coben, D. C. Hammond, M. Arns, 19 channel z-score and LORETA neurofeedback: Does the evidence support the hype, *Appl. Psychophysiol. Biofeedback*, **44** (2019), 1–8. https://doi.org/10.1007/s10484-018-9420-6
12. C. Wei, K. Lou, Z. Wang, M. Zhao, D. Mantini, Q. Liu, Edge sparse basis network: A deep learning framework for EEG source localization, in *2021 International Joint Conference on Neural Networks (IJCNN)*, (2021), 1–8. https://doi.org/10.1109/IJCNN52387.2021.9533968
13. Z. Jiang, Y. Liu, W. Li, Y. Dai, L. Zou, Integration of simultaneous fMRI and EEG source localization in emotional decision problems, *Behav. Brain Res.*, **448** (2023), 114445. https://doi.org/10.1016/j.bbr.2023.114445
14. S. M. Sadjadi, E. Ebrahimzadeh, M. Shams, M. Seraji, H. S. Zadeh, Localization of epileptic foci based on simultaneous EEG–fMRI data, *Front. Neurol.*, **12** (2021), 645594. https://doi.org/10.3389/fneur.2021.645594
15. N. Moradi, B. G. Goodyear, R. C. Sotero, Deep EEG source localization via EMD-based fMRI high spatial frequency, *Plos One*, **19** (2024), e0299284. https://doi.org/10.137/journal.pone.0299284
16. J. Riffi, A. M. Mahraz, A. Abbad, H. Tairi, 3D extension of the fast and adaptive bidimensional empirical mode decomposition, *Multidimens. Syst. Signal Process.*, **26** (2015), 823–834. https://doi.org/10.1007/s11045-014-0283-6
17. T. Nguyen, T. Zhou, T. Potter, L. Zou, Y. Zhang, The cortical network of emotion regulation: Insights from advanced EEG-fMRI integration analysis, *IEEE Trans. Med. Imaging*, **38** (2019), 2423–2433. https://doi.org/10.1109/TML.2019.2900978
18. B. Wang, A. D. N. Initiative, Enhanced brain efficiency network by integrating the new causality with fMRI and its application for Alzheimer's disease study, *Biomed. Signal Process. Control*, **86** (2023), 105364. https://doi.org/10.1016/j.bspc.2023.105364
19. S. N. Kalburgi, T. Kleinert, D. Aryan, K. Nash, B. Schiller, T. Koenig, MICROSTATELAB: The EEGLAB Toolbox for resting-state Microstate Analysis, *Brain Topogr.*, **37** (2023), 621–645. https://doi.org/10.1007/s10548-023-01003-5

20. M. Amann, M. Andelova, A. Pfister, N. M. Lenke, S. Traud, J. Reinhardt, et al., Subcortical brain segmentation of two dimensional T1-weighted data sets with FMRIB's Integrated Registration and Segmentation Tool (FIRST), *NeuroImage Clin.*, **7** (2015), 43–52. https://doi.org/10.1016/j.nicl.2014.11.010
21. R. K. Niazy, G. Iannetti, C. F. Beckmann, M. Brady, S. M. Smith, Improved FMRI artifact reduction from simultaneously acquired EEG data using slice dependant template matching, *NeuroReport*, **80** (1999).
22. C. Yan, X. Wang, X. Zuo, Y. Zang, DPABI: Data processing & analysis for (resting-state) brain imaging, *Neuroinformatics*, **14** (2016), 339–351. https://doi.org/10.1007/s12021-016-9299-4
23. A. Agosstini, F. Benuzzi, D. Ballotta, F. Rizzello, P. Gionchetti, N. Filippini, Differential brain structural and functional patterns in Crohn's disease patients are associated with different disease stages, *Inflammatory Bowel Dis.*, **29** (2023), 1297–1305. https://doi.org/10.1093/ibd/izad029
24. J. Deng, J. Sun, S. Lu, K. Yue, W. Li, H. Shi, et al., Exploring neural activity in inflammatory bowel diseases using functional connectivity and DKI-fMRI fusion, *Behav. Brain Res.*, **443** (2023), 114325. https://doi.org/10.1016/j.bbr.2023.114325
25. K. Friston, L. Harrison, J. Daunizeau, S. Kiebel, C. Phillips, N. T. Barreto, et al., Multiple sparse priors for the M/EEG inverse problem, *NeuroImage*, **39** (2008), 1104–1120. https://doi.org/10.1016/j.neuroimage.2007.09.048
26. X. Lei, Electromagnetic brain imaging based on standardized resting-state networks, in *2012 5th International Conference on BioMedical Engineering and Informatics*, (2012), 40–44. https://doi.org/10.1109.BMEI.2012.6512901
27. K. Friston, J. Mattout, N. T. Barreto, J. Ashhburner, W. Penny, Variational free energy and the Laplace approximation, *NeuroImage*, **34** (2007), 220–234. https://doi.org/10.1016/j.neuroimage.2006.08.035
28. N. J. T. Barreto, E. A. Vazquez, W. D. Penny, Bayesian M/EEG source reconstruction with spatio-temporal priors, *NeuroImage*, **39** (2008), 318–335. https://doi.org/10.1016/j.neuroimage.2007.07.062
29. R. N. Henson, D. G. Wakeman, V. Litvak, K. J. Friston, A parametric empirical Bayesian framework for the EEG/MEG inverse problem: generative models for multi-subject and multi-modal integration, *Front. Hum Neurosci.*, **5** (2011), 76. https://doi.org/10.3389/fnhum.2011.00076
30. X. Geng, X. Fan, Y. Zhong, M. F. Casanova, E. M. Sokhadze, X. Li, et al., Abnormalities of EEG functional connectivity and effective connectivity in children with autism spectrum disorder, *Brain Sci.*, **13** (2023), 130. https://doi.org/10.3390/brainsci13010130
31. J. Vorwerk, C. H. Wolters, D. Baumgarten, Global sensitivity of EEG source analysis to tissue conductivity uncertainties, *Front. Hum. Neurosci.*, **18** (2024), 1335212. https://doi.org/10.3389/fnhum.2024.1335212
32. S. J. Vogrin, C. Plummer, EEG source imaging—clinical considerations for EEG acquisition and signal processing for improved temporo-spatial resolution, *J. Clin. Neurophysiol.*, **41** (2024), 8–18. https://doi.org/10.1097/WNP.0000000000001023
33. G. Lin, A. Lin, Y. Mi, D. Gu, Measurement of information transfer based on phase increment transfer entropy, *Chaos Soliton. Fract.*, **174** (2023), 113864. https://doi.org/10.1016/j.chaos.2023.113864

34. G. Chiarion, L. Sparacino, Y. Antonacci, L. Faes, L. Mesin, Connectivity analysis in EEG data: A tutorial review of the state of the art and emerging trends, *Bioengineering*, **10** (2023), 372. https://doi.org/10.3390/bioengineering10030372
35. A. Ekhlasi, A. M. Nasrabadi, M. Mohammadi, Classification of the children with ADHD and healthy children based on the directed phase transfer entropy of EEG signals, *Front. Biomed. Technol.*, **8** (2021). https://doi.org/10.18502/fbt.v8i2.6515
36. C. Jao, C. I. Lau, L. Lien, Y. Tsai, K. Chu, C. Hsiao, et al., Using fractal dimension analysis with the Desikan–Killiany atlas to assess the effects of normal aging on subregional cortex alterations in adulthood, *Brain Sci.*, **11** (2021), 107. https://doi.org/10.3390/brainsci11010107
37. A. Z. Snyder, Intrinsic brain activity and resting state networks, *Neurosci. in the 21st century*, **2022** (2022), 1939–1990. https://doi.org/10.1007/978-3-030-88832-9_133
38. R. Abreu, J. F. Soares, A. C. Lima, L. Sousa, S. Batista, M. C. Branco, et al., Optimizing EEG source reconstruction with concurrent fMRI-derived spatial priors, *Brain Topogr.*, **35** (2022), 282–301. https://doi.org/10.1007/s10548-022-00891-3
39. A. Ojeda, K. K. Delgado, T. Mullen, Fast and robust block-sparse Bayesian learning for EEG source imaging, *NeuroImage*, **174** (2018), 449–462. https://doi.org/10.1016/j.neuroimage.2018.03.048
40. X. Lei, P. Xu, C. Luo, J. Zhao, D. Zhou, D. Yao, fMRI functional networks for EEG source imaging, *Hum. Brain Mapp.*, **32** (2011), 1141–1160. https://doi.org/10.1002/hbm.21098
41. S. Yang, M. B. Reveret, Y. J. Choo, M. C. Chang, Association between chronic pain and alterations in the mesolimbic dopaminergic system, *Brain Sci.*, **10** (2020), 701. https://doi.org/10.3390/brainsci10100701
42. Y. S. Liaw, G. J. Augustine, The claustrum and consciousness: An update, *Int. J. Clin. Health Psychol.*, **23** (2023), 100405. https://doi.org/10.1016/j.ijchp.2023.100405
43. D. Zhong, K. Jin, R. Wang, B. Chen, J. Zhang, C. Ren, et al., Microalgae-based hydrogel for inflammatory bowel disease and its associated anxiety and depression, *Adv. Mater.*, **36** (2024), 2312275. https://doi.org/10.1002/adma.202312275
44. Y. Yang, T. Wei, W. Yang, S. Hu, H. Jiang, W. Dong, et al., Dysfunction of the lenticular nucleus is associated with dystonia in Wilson's disease, *Brain Sci.*, **13** (2022), 7. https://doi.org/10.3390/brainsci13010007
45. B. C. Duchesne, L. T. Stike, G. I. Zubicaray, K. L. McMahon, P. M. Thompson, I. B. Hickie, et al., Lingual gyrus surface area is associated with anxiety-depression severity in young adults: A genetic clustering approach, *Eneuro*, **5** (2018). https://doi.org/10.1523/ENEURO.0153-17.2017
46. C. Koutsarnakis, S. Komaitis, E. Drosos, A. V. Kalyvas, G. P. Skandalakis, F. Liakos, et al., Mapping the superficial morphology of the occipital lobe: Proposal of a universal nomenclature for clinical and anatomical use, *Neurosurg. Rev.*, **44** (2021), 335–350. https://doi.org/10.1007/s10143-019-01212-2
47. S. Smerconish, J. E. Schmitt, Neuroanatomical correlates of cognitive dysfunction in 22q11.2 deletion syndrome, *Genes*, **15** (2024), 440. https://doi.org/10.3390/genes15040440
48. A. Ogura, H. Watanabe, K. Kawabata, R. Ohdake, Y. Tanaka, M. Masuda, et al., Semantic deficits in ALS related to right lingual/fusiform gyrus network involvement, *EBioMedicine*, **47** (2019), 506–517. https://doi.org/10.1016/j.ebiom.2019.08.022

49. N. Aldusary, G. L. Taber, P. Freund, F. C. Fierz, K. P. Weber, A. Baeshhen, et al., Abnormal connectivity and brain structure in patients with visual snow, *Front. Hum. Neurosci.*, **14** (2020), 582031. https://doi.org/10.3389/fnhum.2020.582031

AIMS Press